Structural perfection and the electrical and magnetic responses of icosahedral AlPdMn quasicrystals

M. Klanjšek,[1] P. Jeglič,[1] P. McGuiness,[1] M. Feuerbacher,[2] E. S. Zijlstra,[3] J. M. Dubois,[4] and J. Dolinšek[1]
[1]*J. Stefan Institute, University of Ljubljana, Jamova 39, SI-1000 Ljubljana, Slovenia*
[2]*Institut für Festkörperforschung, Forschungszentrum Jülich, D-52425 Jülich, Germany*
[3]*Max-Planck-Institut für Festkörperforschung, Heisenbergstrasse 1, D-70569 Stuttgart, Germany*
[4]*Laboratoire de Science et Génie des Matériaux et de Métallurgie (UMR 7584), Centre d'Ingénierie des Matériaux, Ecole des Mines, Parc de Saurupt, F-54042 Nancy, France*

(Received 20 February 2003; revised manuscript received 28 May 2003; published 20 October 2003)

According to reports in the literature, icosahedral *i*-AlPdMn quasicrystalline samples of a similar composition can exhibit very different magnetic and electrical properties, for example, the spin-glass state, the Kondo compensation of Mn magnetic moments, diamagnetism, and the maximum and minimum in the electrical resistivity. In order to shed light on the origin of these differences, we performed x-ray diffraction (XRD), electrical resistivity, magnetic susceptibility, and nuclear magnetic resonance (NMR) relaxation studies on three *i*-AlPdMn samples with high structural quasiperiodic order that were grown by two different techniques—the Czochralski and the self-flux. The measured parameters—the resistivity with its negative temperature coefficient, the fraction of magnetic Mn atoms, and the partial *s*-state electronic density of states (*s*-DOS)—of the investigated samples were found to be quite different, despite their comparable XRD-determined structural qualities. The Czochralski-grown samples were found to be less magnetic and more resistive than the self-flux-grown sample. The amount of magnetic Mn atoms increases with the increased metallic character of the samples. The NMR-determined *s*-DOS at the Fermi energy was compared to a theoretical *ab initio* calculation for an $Al_{71}Pd_{21}Mn_8$ approximant, and good agreement was found. Our results are in qualitative agreement with the previously observed empirical trend that high resistivity is associated with high structural quality of the *i*-AlPdMn quasicrystals, but the observed small differences in the structural perfection of the investigated samples do not give convincing support to the hypothesis that this could be the main origin of the large differences in the electrical and magnetic response between the samples.

DOI: 10.1103/PhysRevB.68.134210 PACS number(s): 71.23.Ft, 61.44.Br

I. INTRODUCTION

The electrical and magnetic properties of icosahedral *i*-AlPdMn quasicrystals (QC's) still represent a major and controversial issue. Regarding the magnetic response, it was shown that at room temperature only a small fraction of all the manganese atoms, of the order of 1%, carry magnetic moments, the rest being nonmagnetic.[1,2] The deviation from Curie behavior at low temperatures was reported to occur due to a spin-glass transition[1,2] observed typically below 1 K. In other studies,[3,4] the low-temperature magnetism of *i*-AlPdMn QC's was explained in terms of the Kondo effect, where the Kondo screening of moments was reported to occur below $T_K \approx 0.6-1.2$ K. As the Kondo compensated state is nonmagnetic, it is fundamentally different from the spin-glass state. It was also reported that the fraction of Mn magnetic moments in the *i*-AlPdMn strongly depends on the Mn concentration, whereas thermal annealing decreases the magnetic Mn fraction and drives the system toward a diamagnetic state.[5] It is thus not clear whether universal magnetic behavior of the *i*-AlPdMn QC's exists, relating to their quasiperiodic nature, or whether the behavior is sample-dependent, i.e., whether it depends on the sample's composition and its structural perfection.

A similar variety of results were also reported for the temperature-dependent electrical resistivity $\rho(T)$. In general, the resistivities of *i*-AlPdMn QC's exhibit negative temperature coefficients (NTC's), but the magnitude of the NTC varies considerably among samples. In addition, the $\rho(T)$ in many cases displays a maximum[5–9] between room temperature and 4 K and sometimes also a minimum[6–8] at still lower temperatures. Whereas the maximum in $\rho(T)$ can be explained either by a weak localization of the conduction electrons[10] or by a magnetic effect,[11] the low-temperature minimum was attributed to the Kondo effect.[6] However, it was argued[2] that in good-quality *i*-AlPdMn QC's the Kondo effect could not take place because of the low density of electronic states (DOS) at the Fermi energy (E_F), i.e., due to the pseudogap formation. An especially intriguing feature is the large difference between the electrical resistivities of samples grown by different techniques, such as the Czochralski and the ''self-flux,'' which both produce single-grain crystals of very high structural quality. It was claimed[12,13] that the self-flux technique produces remarkably strain-free crystals with a lower defect density than any other technique. Yet the resistivities of the flux-grown *i*-AlPdMn samples can be several times smaller than those grown by other techniques, suggesting[12] that the previously observed empirical trend that a very high resistivity is associated with the highest quality *i*-AlPdMn QC's may not be generally true. An even more pronounced difference is found in the *i*-AlPdRe family, where the flux-grown samples[14] exhibit resistivities up to two orders of magnitude smaller than the arc-melted samples. In addition, the arc-melted samples exhibit a large

$\rho(T)$ increase upon cooling for factors $\rho_{4\,K}/\rho_{300\,K} \approx 10-200$, whereas for flux-grown samples this factor is much smaller, amounting to 1.2–2.5 only.[14] Here, we are again faced with the question as to which of these features are intrinsic to the quasiperiodicity and which occur due to finite sample quality. In addition, it is not clear why there is such a pronounced difference between the flux-grown samples and those grown by other techniques.

One of the common features of QC's is the pseudogap in the DOS at E_F, which stabilizes the QC structure by reducing the band energy. The anomalously low DOS value at E_F has a profound effect on the electronic transport properties of QC's, where it is considered to be responsible for the large electrical resistivity and the small low-temperature specific heat. As the higher-resistivity samples are more diamagnetic,[5] the pseudogap is also indirectly related to the magnetic response of the *i*-AlPdMn.

In this paper we report on a comparative experimental study of the electrical resistivity, magnetic susceptibility, and NMR relaxation performed on three *i*-AlPdMn samples of high structural quality, but grown by two different crystal-growth techniques—the Czochralski and the self-flux methods. The structural perfection was characterized by x rays and was found to be comparable for all three samples, whereas their $\rho(T)$, the fraction of magnetic Mn atoms, and the partial DOS value at E_F at the aluminum sites (the contribution of *s* states) differ considerably. The comparison of these physical parameters is used to discuss the relation between the structural quality of the samples and their electrical and magnetic response.

II. SAMPLE SELECTION AND X-RAY CHARACTERIZATION

Three icosahedral AlPdMn samples were included in the study. The first sample of composition $Al_{70.5}Pd_{21.2}Mn_{8.3}$ was grown by the Czochralski technique and was ''superannealed'' for 35 days at 800 °C in vacuum. Subsequently we refer to this sample as sCz-$AlPdMn_{8.3}$, in order to emphasize its long annealing period and Czochralski origin. The second sample of composition $Al_{69.6}Pd_{22.1}Mn_{8.3}$ was also Czochralski-grown (referred to as Cz-$AlPdMn_{8.3}$) and annealed for one day at 800 °C in vacuum. The Cz-$AlPdMn_{8.3}$ sample was a small bar cut from a large single crystal prepared from a melt of the composition $Al_{72.4}Pd_{20.5}Mn_{7.1}$. Its real composition was determined to be $Al_{69.6}Pd_{22.1}Mn_{8.3}$. The third sample of composition $Al_{72}Pd_{19.5}Mn_{8.5}$ (referred to as *f*-$AlPdMn_{8.5}$) was grown by the self-flux technique.[12,13]

The two growth techniques employed—the Czochralski and the self-flux techniques—are both powerful methods for the growth of incongruently melting materials (as most of the QC systems are) and both produce single-grain samples of high structural order. In the Czochralski technique, the crystal is essentially unstrained during cooling, so that a high structural perfection can be obtained. Large crystals, up to several cm^3, can be produced and the orientation of the crystal can be controlled via the seed crystal. The advantage of the self-flux technique is that the crystal can grow freely into the almost isothermal melt, leading to strain-free[12,13] samples with a high structural quality that show faceted surfaces according to their growth morphology.

The x-ray diffraction (XRD) measurements were carried out using a Bruker D4 Endeavor diffractometer and Cu $K\alpha$ radiation. Each sample was measured in the range $2\theta = 20° - 70°$ with a step size 0.02° and a measuring time of 4 s. All three samples produced very similar XRD patterns (Fig. 1) with the lines in identical positions. For all three samples it was possible to ascribe all the observed peaks, even the very weak ones that exhibited only a few percent of the intensity of the strongest 2 4 0 $\bar{2}$ 0 4 reflection, to those on the PDF card 48-1437 by Matsuo *et al.*[15] This spectrum was measured from an ingot slowly cooled from 906 to 898 °C for 18 h before being quenched, and the sample is considered high quality. In the following we take it as a reference. The analysis of the XRD spectra of Fig. 1 demonstrates that all three samples consist entirely of grains of the *F*-type icosahedral phase. No additional peaks that could come from secondary phases, either crystalline or quasicrystalline, could be observed in any of our three samples. The sharpness of the XRD lines demonstrates a high degree of long-range order in the QC lattice. The widths of the XRD lines are, within experimental resolution, comparable for all three samples, demonstrating their comparable degree of structural order. However, a tiny difference between the linewidths exists and may be noticed on the diffraction peaks at high angles, which exhibit splitting due to the Cu $K\alpha_1$ and Cu $K\alpha_2$ radiation effect. The inspection of the doublets at angles between 62° and 65° indicates that the lines of the sCz-$AlPdMn_{8.3}$ and Cz-$AlPdMn_{8.3}$ samples are somewhat narrower, exhibiting smaller overlap within the doublets, as compared to the *f*-$AlPdMn_{8.5}$ sample. Qualitatively, this suggests that the flux-grown sample contains more phason disorder than the two Czochralski-grown samples, but the differences are small. Regarding comparison of the spectra with that of the reference sample,[15] the most perfect fit was found for the sCz-$AlPdMn_{8.3}$ sample, which showed a good intensity match. The other two samples exhibited less-good fits in terms of a match of intensities.

The above XRD analysis demonstrates that the quality of all three investigated *i*-AlPdMn samples is comparable to that of the reference sample, exhibiting high structural quasicrystalline order with no secondary phases present. The absence of secondary phases is here claimed within the precision of the XRD experiment and cannot exclude the presence of minute traces of secondary phases that could possibly be detected by more precise chemical methods (which, however, irreversibly destroy the samples). However, our XRD characterization, which was performed on powdered samples, cannot detect other types of defects: the microcracks and voids present in the bulk material and its multigrain structure. These defects can have a profound effect on the transport properties of the material. Preliminary investigations with a scanning electron microscope[16] (SEM) have detected a significant concentration of microvoids with a pentagonal shape (20–30 μm in size and separated by an average distance of about 200 μm) in Cz-$AlPdMn_{8.3}$, whereas these were not detected in the sCz-$AlPdMn_{8.3}$ and *f*-$AlPdMn_{8.5}$ samples.

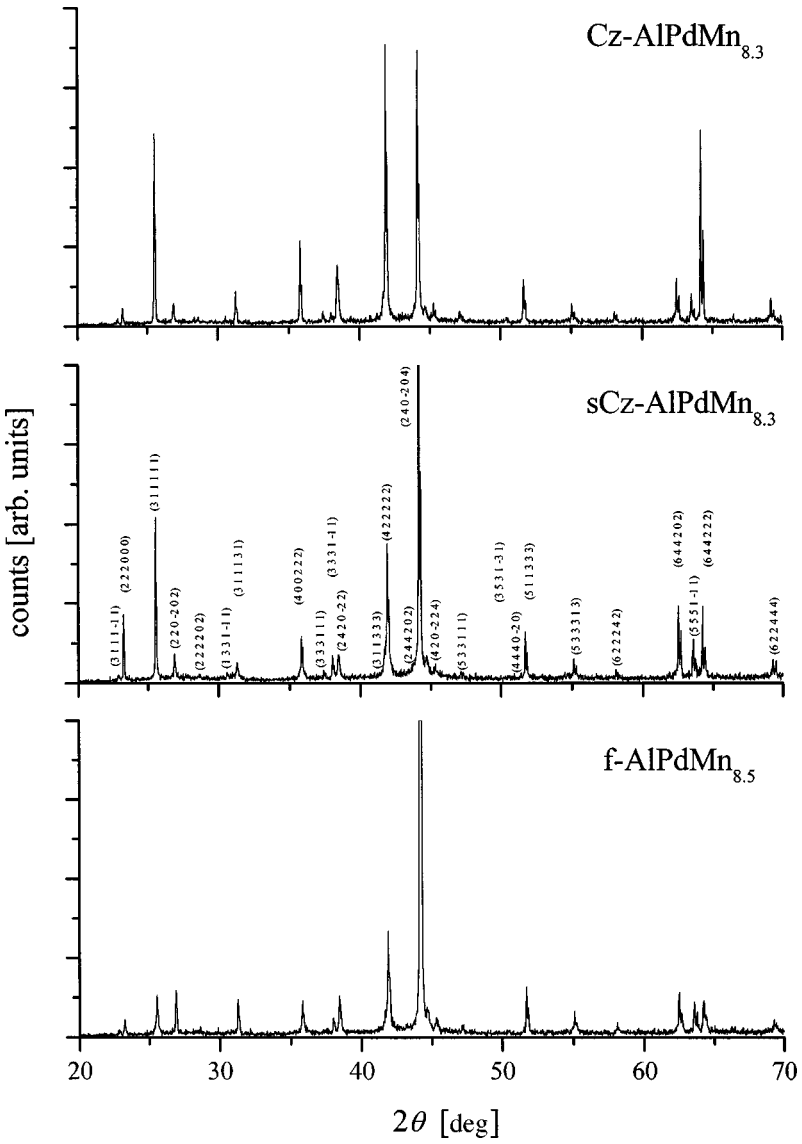

FIG. 1. XRD spectra of the three investigated *i*-AlPdMn samples with the six-dimensional indexing according to Ref. 15.

III. RESULTS

A. Electrical resistivity

The electrical resistivity $\rho(T)$ measurements were performed by a standard four-terminal method in the temperature interval between room temperature and 4 K. The resistivities (Fig. 2) exhibit qualitatively similar temperature dependences by first increasing from room temperature on cooling and then decreasing at low temperatures after passing a maximum. Significant quantitative differences, however, exist. The resistivity of the f-$AlPdMn_{8.5}$ sample is the lowest and at 315 K amounts to $\rho_{315\,K}=1202\ \mu\Omega$ cm. A broad maximum is reached at 120 K where $\rho_{120\,K}=1267\ \mu\Omega$ cm, the total increase from 315 K to the maximum being rather small: $(\rho_{120\,K}-\rho_{315\,K})/\rho_{315\,K}=5\%$. The room-temperature resistivity of the Cz-$AlPdMn_{8.3}$ amounts to $\rho_{290\,K}=2040\ \mu\Omega$ cm. A broad maximum is reached at 160 K, where $\rho_{160\,K}=2046\ \mu\Omega$ cm, the total increase from room temperature to the maximum being practically negligible: $(\rho_{160\,K}-\rho_{290\,K})/\rho_{290\,K}=0.3\%$. The $\rho(T)$ data from these two samples are therefore quite similar (except for the larger overall resistivity of the Cz-$AlPdMn_{8.3}$ sample by a factor of roughly 2): both exhibit a very weak increase on cooling (and hence a small NTC) from room temperature down to the maximum and a significant decrease below this point.

The sCz-$AlPdMn_{8.3}$ sample shows, quite surprisingly, a room-temperature resistivity value intermediate between the previous two samples, $\rho_{300\,K}=1729\ \mu\Omega$ cm. However, its increase on cooling is much stronger: $\rho(T)$ reaches a maximum at 60 K, where $\rho_{60\,K}=2317\ \mu\Omega$ cm, the total increase being $(\rho_{60\,K}-\rho_{300\,K})/\rho_{300\,K}=34\%$. The NTC (the slope) of $\rho(T)$ between room temperature and the maximum is thus much larger in this superannealed sample and the temperature of the maximum is shifted to lower temperatures. It is remarkable that the $\rho(T)$ curve of sCz-$AlPdMn_{8.3}$ even crosses that of Cz-$AlPdMn_{8.3}$ at 180 K.

B. Magnetic susceptibility

The magnetic susceptibility $\chi(T)$ measurements (Fig. 3) were performed in the same temperature range as for $\rho(T)$. Magnetization M was measured in a field $H=1$ T where the

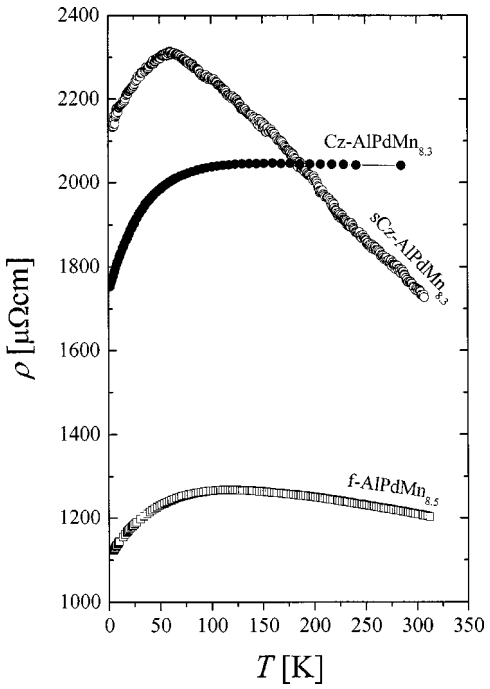

FIG. 2. Temperature-dependent electrical resistivities $\rho(T)$ of three icosahedral *i*-AlPdMn QC's: superannealed sCz-AlPdMn$_{8.3}$ (open circles); Cz-AlPdMn$_{8.3}$ (full circles); flux-grown *f*-AlPdMn$_{8.5}$ (squares).

variation of M with H is still linear, so that we consider the $\chi = M/H$ ratio in the following. χ contains both a diamagnetic and a paramagnetic contribution, which, in the high-temperature regime, can be described by

$$\chi = \chi_d + \frac{C}{T-\theta}. \tag{1}$$

The diamagnetic contribution was estimated from the room-temperature $\chi(T)$ data. For Cz-AlPdMn$_{8.3}$ we obtained $\chi_d = -1.4\times10^{-5}$ emu/mole of sample, which is close to the susceptibility $\chi_d \approx -8\times10^{-6}$ emu/mole of sample calculated from the tabulated values of the atomic core diamagnetic susceptibilities. The data were then analyzed in the form $(\chi-\chi_d)^{-1}$ vs T. The fit with Eq. (1) in the high-temperature regime ($T>50$ K) yielded the Curie-Weiss temperature $\theta=-26$ K and the Curie-Weiss constant $C=3.2\times10^{-2}$ emu K/mole of Mn, from which we obtain the mean effective moment $p_{\rm eff}^{(\rm expt)}=0.51\mu_B/(\text{Mn atom})$. This low $p_{\rm eff}^{(\rm expt)}$ value may be interpreted as an indication that only a fraction f of all the Mn atoms carry localized moments. The mean effective moment per magnetic atom in the regime $k_BT \gg p_{\rm eff}H$ is defined as[17] $p_{\rm eff}=p_{\rm eff}^{(\rm expt)}/\sqrt{f}$, so that the true mean effective moment $p_{\rm eff}$ is larger than the experimentally measured value $p_{\rm eff}^{(\rm expt)}$ by a factor $1/\sqrt{f}$. For the *i*-AlPdMn system the actual valence of the Mn atoms is not known, but the $p_{\rm eff}$ values for the three most likely configurations of the Mn ions[18] are all relatively close to $5\mu_B$, i.e., $p_{\rm eff}(Mn^{2+})=5.9\mu_B$, $p_{\rm eff}(Mn^{3+})=5.0\mu_B$, and $p_{\rm eff}(Mn^{4+})=4.0\mu_B$. Assuming that the nonzero Mn moments have an average value $p_{\rm eff}\approx5\mu_B$, we derive a fraction $f=(p_{\rm eff}^{(\rm expt)}/p_{\rm eff})^2=1.0\%$ of all Mn atoms in the Cz-AlPdMn$_{8.3}$ sample that carry magnetic moments within the analyzed temperature range. Our analysis thus interprets the high-temperature susceptibility as indicating that only a small fraction, 1%, of all the Mn atoms carries localized magnetic moments and that these moments have the full magnitude expected for manganese. An identical analysis was also performed on the $\chi(T)$ data of the sCz-AlPdMn$_{8.3}$ and the *f*-AlPdMn$_{8.5}$ samples. For the sCz-AlPdMn$_{8.3}$ we obtained $p_{\rm eff}^{(\rm expt)}=0.31\mu_B/(\text{Mn atom})$, so that a fraction $f=0.4\%$ of all Mn atoms is magnetic in that sample. This is, roughly by a factor of 2, smaller than the Cz-AlPdMn$_{8.3}$. For the *f*-AlPdMn$_{8.5}$, on the other hand, we obtained $p_{\rm eff}^{(\rm expt)}=1.1\mu_B/(\text{Mn atom})$, yielding a much larger Mn magnetic fraction $f=4.8\%$. The small fractions of magnetic Mn atoms of about 1% in the investigated Cz-AlPdMn$_{8.3}$ and sCz-AlPdMn$_{8.3}$ samples are consistent with the f values determined from the specific heat and magnetic susceptibility measurements on some other *i*-AlPdMn samples,[1,2] whereas the magnetic fraction $f=4.8\%$ of the *f*-AlPdMn$_{8.5}$ appears quite large within the *i*-AlPdMn family. The Curie-type temperature dependence of $\chi(T)$ presented in Fig. 3 also demonstrates that the Mn moments are localized.

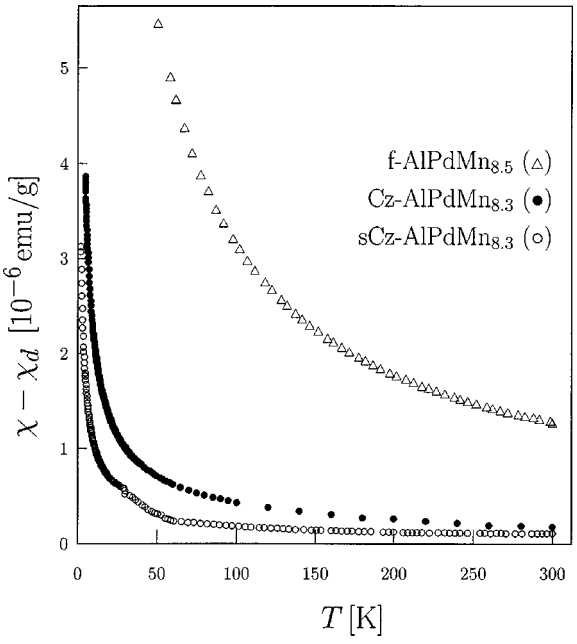

FIG. 3. Temperature-dependent paramagnetic susceptibilities $\chi-\chi_d$ of the superannealed sCz-AlPdMn$_{8.3}$ (open circles), Cz-AlPdMn$_{8.3}$ (full circles), and flux-grown *f*-AlPdMn$_{8.5}$ (triangles).

C. NMR spin-lattice relaxation

The NMR spin-lattice relaxation rate of the QC's was studied before in detail, both theoretically[19,20] and experimentally.[19–23] For the *i*-AlPdMn QC's the ^{27}Al relaxation rate can be, to a good approximation, taken as a sum of the conduction-electron rate T_{1c}^{-1} and the paramagnetic rate

T_{1P}^{-1} due to spin diffusion via paramagnetic Mn centers.[19] The conduction-electron relaxation rate is written as[23,19]

$$\frac{1}{\beta_s T_{1c}} = g_0^2 k_B T + g_0 g_0'' \frac{\pi^2}{3} (k_B T)^3. \quad (2)$$

Here $g_0 = g(E_F)$ is the electronic DOS at E_F, $g_0'' = (\partial^2 g/\partial E^2)_{E_F}$ is the second derivative of the DOS, $\beta_s = 64/9\pi^3 \hbar^3 \gamma_e^2 \gamma_n^2 \langle |u_k(0)|^2 \rangle_{E_F}^2$ is the proportionality constant, γ_e and γ_n are the electron and the nuclear gyromagnetic ratios, and $\langle |u_k(0)|^2 \rangle_{E_F}$ is the density of the electronic wave function at the nucleus averaged over the Fermi surface. The linear-in-T term in Eq. (2) represents the usual Korringa metallic relaxation, whereas the T^3 term originates from the variation of the DOS ($g_0'' \neq 0$) in the vicinity of the E_F due to the existence of the pseudogap. It should be pointed out that Eq. (2) is derived for the case where the Fermi contact interaction between conduction-*s*-electron spins and the nuclear spins dominates the spin-lattice relaxation. This contribution is usually very dominant in metallic samples where at least a fraction of the conduction electrons exhibit *s* character. The DOS parameters g_0 and g_0'' in Eq. (2) thus refer to the partial *s*-state DOS.

In the *i*-AlPdMn QC's an important nuclear relaxation mechanism at low temperatures comes from the relaxation via localized paramagnetic Mn centers in combination with spin diffusion[19] (recall that a fraction of the order of 1% of all Mn atoms are magnetic). Assuming that the paramagnetic electronic fluctuations are fast on the nuclear Larmor frequency scale, the paramagnetic relaxation rate depends on the longitudinal electronic relaxation time τ as[24] $T_{1P}^{-1} \propto \tau^{1/4}$. In diluted paramagnets, where the interaction between electronic moments is negligible, τ normally does not exhibit pronounced temperature dependence, so that T_{1P}^{-1} is, to a good approximation, temperature-independent. Correlations between electrons introduce an implicit temperature dependence into τ, a typical example being the slowing-down dynamics of the electronic fluctuations at low temperatures on approaching a cooperative magnetic phase transition or a spin-glass state. There the $\tau(T)$ dependence introduces a temperature dependence into the paramagnetic rate $T_{1P}^{-1}(T)$. Since the temperature dependence of the electronic relaxation time τ in our samples is not known, we assume that the paramagnetic rate obeys a power-law temperature dependence, $T_{1P}^{-1} = d/T^m$, as empirically observed[20] in the *i*-AlPdMn and *i*-AlCuFe QC's. Here, the power-law exponent *m* is considered as an experimental fit parameter and the T_{1P}^{-1} fits with this empirical form should be considered as qualitative only. As our analysis of the electronic DOS shall be performed on the conduction-electron relaxation rate, the exact microscopic model of the paramagnetic relaxation, which only becomes dominant at low temperatures, is of minor importance.

In order to emphasize the difference between QC's and regular metals, the total relaxation rate T_1^{-1} is best analyzed in the form of a $(T_1T)^{-1}$-vs-T plot, which yields for regular metals a horizontal $(T_1T)^{-1} = \text{const}$ line. We shall perform the analysis with the expression[19]

$$\frac{1}{T_1T} = a + bT^2 + \frac{d}{T^{1+m}}, \quad (3)$$

where $a = \beta_s k_B g_0^2$ and $b = \beta_s g_0 g_0'' (\pi^2/3) k_B^3$ are the parameters of the conduction-electron relaxation rate and *d* and *m* refer to the paramagnetic rate. In Eq. (3) we neglected the electric quadrupolar contribution to the relaxation of quadrupolar nuclei such as ^{27}Al. It was shown[21] that the quadrupolar relaxation in *i*-AlPdMn QC's is also observable but of lesser importance than the conduction-electron and the paramagnetic terms. The dominant *s*-type relaxation due to electron-nucleus hyperfine magnetic coupling was also confirmed in the *i*-AlCuFe(Ru) by inspecting the $T_1(^{65}\text{Cu})/T_1(^{63}\text{Cu})$ ratio.[22]

The NMR spin-lattice relaxation experiments were performed on ^{27}Al (spin $\frac{5}{2}$) nuclei in the temperature interval from 300 to 4 K at the resonance frequency $\nu_0(^{27}\text{Al}) = 26.134$ MHz. The measurements were performed on the central $(\frac{1}{2} \leftrightarrow -\frac{1}{2})$ nuclear spin transition. The saturation-recovery pulse sequence was employed with a saturation train of 60 $\pi/2$ pulses of 2 μsec duration. The spin-lattice relaxation rate T_1^{-1} was extracted from the magnetization-recovery curves by the long-saturation magnetic relaxation model of Narath.[25]

The relaxation data are displayed in Fig. 4. The *f*-AlPdMn$_{8.5}$ sample exhibits from 300 to 30 K an almost perfect Korringa-type $T_1T = \text{const} \approx 40$ K s dependence, where the second derivative of the DOS g_0'' is practically zero. This demonstrates that the DOS $g(E)$ function in the vicinity of the E_F is not changing noticeably, resembling the situation in regular metals. The *f*-AlPdMn$_{8.5}$ thus exhibits a quite significant metallic character. The increase of $(T_1T)^{-1}$ below 30 K is caused by the paramagnetic relaxation via the magnetic Mn atoms that starts to dominate over the conduction-electron relaxation mechanism at low temperatures. The T_1T data were reproduced by Eq. (3) (solid line in Fig. 4) using the fit parameters $a = (2.54 \pm 0.15) \times 10^{-2}$ K^{-1} s^{-1}, $b = 0$, $d = 455 \pm 20$ s^{-1} (where the temperature in the paramagnetic relaxation contribution $T_{1P}^{-1} = d/T^m$ is considered dimensionless), and $m = 2.7$. From the parameter $a = \beta_s k_B g_0^2$ we may estimate the reduction of the partial *s*-state DOS at the E_F of the *f*-AlPdMn$_{8.5}$ with respect to the partial *s*-state DOS of metallic aluminum (99.999% purity bulk sample), the relaxation data of which are also displayed in Fig. 4. Pure aluminum is a free-electron-like metal and its NMR relaxation rate exhibits a perfect Korringa law[26] $(T_1T)_{\text{Al}} = 1.88$ K s. The reduction of g_0 in the *f*-AlPdMn$_{8.5}$ with respect to the metallic Al is then obtained from $g_0/g_0(\text{Al}) = \sqrt{a(T_1T)_{\text{Al}}}$, where $(T_1T)_{\text{Al}}^{-1} = \beta_s k_B g_0^2(\text{Al})$ and we adopted the previously used approximation[19] that the proportionality constant β_s is the same for the metallic Al as well as for the investigated QC's. Within this approximation we obtain $g_0/g_0(\text{Al}) = 0.22$, which estimates the g_0 of the *f*-AlPdMn$_{8.5}$ to be reduced to 22% of that of the metallic Al.

The $(T_1T)^{-1}$ data of the Cz-AlPdMn$_{8.3}$ sample (Fig. 4) no longer follow the simple Korringa $T_1T = \text{const}$ law at high temperature, but exhibit a continuous decrease from 300 to

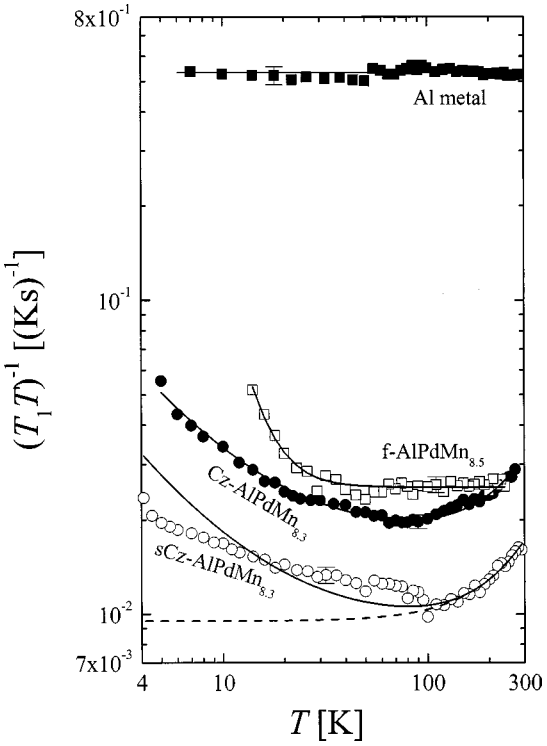

FIG. 4. Temperature-dependent ^{27}Al NMR spin-lattice relaxation rates of the three *i*-AlPdMn samples in a $(T_1T)^{-1}$ vs T plot (open circles, superannealed sCz-AlPdMn$_{8.3}$ sample; full circles, Cz-AlPdMn$_{8.3}$; open squares, flux-grown f-AlPdMn$_{8.5}$). Solid lines represent the fits with Eq. (3); dashed line shows only the conduction-electron relaxation contribution for the sCz-AlPdMn$_{8.3}$. The $(T_1T)^{-1}$ data of the fcc metallic aluminum (full squares) are shown for comparison. The T_1 of the QC samples was extracted from the magnetization-recovery curves by the long-saturation model of Narath (Ref. 25), whereas for the metallic aluminum it was extracted from the simple monoexponential model $M(t) = M_0[1-\exp(-t/T_1)]$ due to Al cubic symmetry.

about 80 K, where a shallow minimum is observed. Below the minimum $(T_1T)^{-1}$ starts to increase toward low temperatures due to the domination of the paramagnetic relaxation term. As compared to the f-AlPdMn$_{8.5}$ sample, two important differences are noticed in the conduction-electron relaxation contribution (that dominates above 80 K) of the Cz-AlPdMn$_{7.1}$. First, is the nonzero slope of $(T_1T)^{-1}$ above 80 K, which reflects the nonzero second derivative g_0'' and hence a steeper variation of the DOS (the pseudogap) in the vicinity of the E_F in this sample. Second is the overall smaller value of the $(T_1T)^{-1}$, which demonstrates a lower g_0 value. The fit procedure with Eq. (3) (solid line in Fig. 4) yielded the parameter values $a=(1.7\pm0.1)\times10^{-2}$ K^{-1} s^{-1}, $b=(1.58\pm0.1)\times10^{-7}$ K^{-3} s^{-1}, $d=0.17\pm0.004$ s^{-1}, and $m\approx0$ (equally good fits could be obtained for m between 0 and 0.25), from which we find the ratio $g_0/g_0(\mathrm{Al})=0.18$, slightly lower than that in the more metallic f-AlPdMn$_{8.5}$. From the parameters a and b the ratio $g_0''/g_0=3b/(a\pi^2k_B^2)$ could also be determined, which for the Cz-AlPdMn$_{8.3}$ amounts to 384 eV^{-2}.

The $(T_1T)^{-1}$ data of the sCz-AlPdMn$_{8.3}$ sample (Fig. 4) exhibit the minimum at 100 K and the smallest overall $(T_1T)^{-1}$ values, demonstrating that the pseudogap in this sample is the deepest. The fit (solid line in Fig. 4) yielded the conduction-electron relaxation rate parameters $a=(8.82\pm0.3)\times10^{-3}$ K^{-1} s^{-1} and $b=(8.97\pm0.4)\times10^{-8}$ K^{-3} s^{-1}, with the ratios $g_0/g_0(\mathrm{Al})=0.13$ and $g_0''/g_0=416$ eV^{-2}. The $g_0/g_0(\mathrm{Al})=13\%$ ratio of the sCz-AlPdMn$_{8.3}$ is the smallest among the three investigated samples. Below the minimum the fit with Eq. (3) (solid line) does not reproduce well the $(T_1T)^{-1}$ data of this sample, indicating that the simple power-law form d/T^m of the paramagnetic relaxation rate is here not a good approximation. A qualitative fit was obtained with $d=(9.5\pm0.15)\times10^{-2}$ s^{-1} and $m=0$. In order to demonstrate the almost negligible effect of the paramagnetic relaxation at temperatures above the $(T_1T)^{-1}$ minimum, the conduction-electron rate is shown separately by a dashed line. It is seen that above 100 K the total rate (solid line) is practically indistinguishable from the conduction-electron rate (dashed line).

The above partial *s*-state DOS values at the E_F of the *i*-AlPdMn samples, which are related to the degree of their metallic character, thus differ quite significantly. The obtained $g_0/g_0(\mathrm{Al})$ values in the range 0.13–0.22 are consistent with the value $g_0/g_0(\mathrm{Al})=0.12$ determined for the *i*-AlCuRu by a similar NMR relaxation experiment.[23] Our g_0''/g_0 values of about 400 eV^{-2} also agree with that of the *i*-AlCuRu, where an estimated value of 500 eV^{-2} was reported.[23]

IV. DISCUSSION

In order to get a quantitative insight into the NMR-determined partial *s*-state DOS value at E_F we compared the experimental $g_0/g_0(\mathrm{Al})$ values in the range 0.13–0.22 to the theoretical expectations, which we obtained by performing an *ab initio* electronic structure calculation of the total and partial DOS of an $Al_{71}Pd_{21}Mn_8$ approximant using the relaxed structural model of Quandt and Elser[27] with the exact *Immm* symmetry.[28] We used the linear muffin-tin orbital (LMTO) method,[29,30] and the details of the calculation are given in Table I. The same method was used to calculate the DOS of pure metallic fcc Al, yielding the following values: total DOS at E_F 0.40, partial *s*-DOS 0.085, *p*-DOS 0.194, *d*-DOS 0.118 (all in units states/eV atom). Using an effective tight-binding (TB) Hamiltonian based on a fit of the band structure calculated by the augmented plane wave (APW) method, the theoretical DOS of metallic fcc Al is[31] total DOS at E_F, 0.40; partial *s*-DOS, 0.14; *p*-DOS, 0.23; *d*-DOS, 0.026 (all in units states/eV atom). The total DOS value is the same as the one obtained by our LMTO calculation. The subdivision of the total DOS into partial DOS contributions depends on the choice of the basis-set wave functions and is therefore method dependent. For that reason the partial DOS values obtained from the LMTO method and the effective TB Hamiltonian differ slightly. For a proper comparison of the $Al_{71}Pd_{21}Mn_8$ approximant to the fcc Al we used the partial DOS values calculated by the same method (LMTO). The calculated DOS for the $Al_{71}Pd_{21}Mn_8$ approximant (the model crystal containing 65 atoms in the unit cell, 14.561 Å^3

TABLE I. Fractional coordinates (x, y, z) for the relaxed Quandt-Elser model (Ref. 27) with exact *Immm* symmetry. The unit cell is spanned by the vectors $(a,0,0)$, $(0,b,0)$, and $(a/2,b/2,c/2)$, with $a=7.138$ Å, $b=12.945$ Å, and $c/2=10.242$ Å. The Cartesian atomic coordinates of the atoms are $\vec{\mathbf{r}}=(xa,yb,zc/2)$. The positions of the empty spheres that were used in the LMTO calculation are given in the last eleven rows of the table. The last two columns give the atomic sphere radii r_s and the basis states used in the calculation.

Class	Multiplicity	x	y	z	r_s (Å)	Basis
Al_0	4	0	0.3151	0.4916	1.460	*spd*
Al_1	4	0.5	0.1831	0.2438	1.510	*spd*
Al_2	4	0.1880	0.5	0.3727	1.472	*spd*
Al_3	4	0.3148	0	0.1612	1.373	*spd*
Al_4	8	0.1919	0.1138	0.3819	1.460	*spd*
Al_5	1	0	0.5	0	1.374	*spd*
Al_6	1	0	0	0	1.403	*spd*
Al_7	8	0.3070	0.3907	0.1266	1.367	*spd*
Al_8	8	0.1781	0.1846	0.1236	1.480	*spd*
Al_9	4	0	0.3498	0.2402	1.522	*spd*
Pd_0	2	0.5	0.5	0.4787	1.422	*spdf*
Pd_1	2	0.5	0.1161	0	1.580	*spdf*
Pd_2	8	0.2963	0.3065	0.3683	1.421	*spdf*
Pd_3	2	0.5	0	0.3916	1.635	*spdf*
Mn_0	2	0	0.3170	0	1.395	*spd*
Mn_1	2	0	0	0.2335	1.391	*spd*
Mn_2	1	0.5	0.5	0	1.393	*spd*
E_0	2	0.5	0.5	0.2469	1.352	*spd*
E_1	2	0.5	0.3014	0	1.224	*spd*
E_2	4	0.1299	0.5	0.1761	0.928	*sp*
E_3	4	0.5	0.3422	0.2445	0.896	*sp*
E_4	4	0	0.1929	0.2780	0.894	*sp*
E_5	4	0.5	0.3410	0.4889	0.868	*sp*
E_6	4	0.2585	0.2902	0	0.798	*sp*
E_7	4	0.2263	0.0739	0	0.791	*sp*
E_8	2	0	0.1405	0	0.721	*s*
E_9	4	0.5	0.3944	0.3611	0.707	*s*
E_{10}	2	0.2488	0.5	0	0.695	*s*

volume per atom) is displayed in Fig. 5. The DOS exhibits a pronounced pseudogap in the vicinity of the Fermi level with the following total and partial DOS values at the E_F: total DOS 0.130, partial *s*-DOS 0.010, *p*-DOS 0.048, *d*-DOS 0.063 (all in states/eV atom). The contributions to the partial DOS's in the empty spheres (see Table I) are not included in the above values and for that reason the partial DOS's do not sum up precisely to the total DOS value. The theoretical reduction of the *s*-DOS in the $Al_{71}Pd_{21}Mn_8$ approximant with respect to the fcc Al thus amounts to $g_0/g_0(\mathrm{Al})=0.12$, which compares well to the experimental values (0.13 for the sCz-$AlPdMn_{8.3}$ sample up to 0.22 for the f-$AlPdMn_{8.5}$).

The combination of the above electrical resistivity, magnetic susceptibility, and NMR relaxation experiments allows us to draw the following correlations between the $\rho(T)$, the number of Mn magnetic moments and the partial *s*-DOS. The

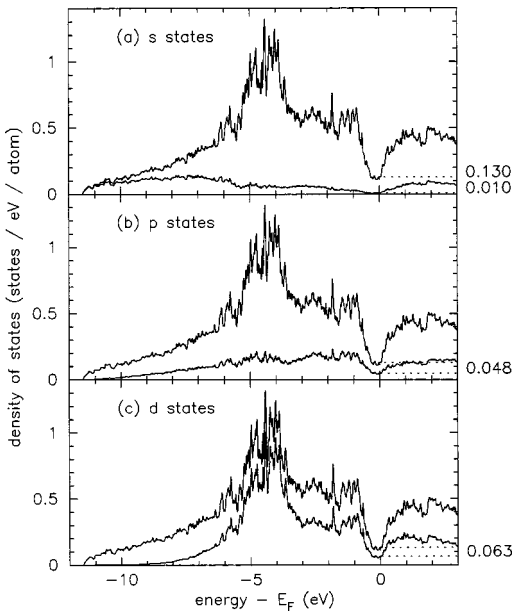

FIG. 5. Theoretical electronic DOS calculated for the $Al_{71}Pd_{21}Mn_8$ approximant using the model of Quandt and Elser (Ref. 27). In each panel the upper curve represents the total DOS, whereas the lower curve is the partial atomic (a) *s*-DOS, (b) *p*-DOS, and (c) *d*-DOS contribution. The respective values at the Fermi level (chosen as the energy scale origin) are also given.

sCz-$AlPdMn_{8.3}$ sample contains the smallest magnetic Mn fraction $f=0.4\%$, the smallest *s*-state DOS $[g_0/g_0(\mathrm{Al})=0.13]$ and the largest NTC of the resistivity. The Cz-$AlPdMn_{8.3}$ contains an intermediate magnetic fraction $f=1\%$, an intermediate *s*-DOS $[g_0/g_0(\mathrm{Al})=0.18]$ and a very small $\rho(T)$ NTC. The f-$AlPdMn_{8.5}$ contains the largest magnetic fraction $f=4.8\%$, the largest *s*-DOS $[g_0/g_0(\mathrm{Al})=0.22]$ but again with a small NTC. This strongest magnetic sample also exhibits the smallest absolute value of the resistivity, whereas the resistivities of the other two samples are comparable and about a factor of 2 larger. At low temperatures, the least magnetic sCz-$AlPdMn_{8.3}$ exhibits the highest resistivity.

Regarding the magnetic response, the magnetic Mn fractions increase in the order sCz-$AlPdMn_{8.3}$ → Cz-$AlPdMn_{8.3}$ → f-$AlPdMn_{8.5}$. Together with the increasingly larger *s*-state DOS value at E_F and the decreasing electrical resistivity in the same order of samples this indicates that the enhanced magnetism follows the increased metallic character of the samples. This conclusion is in agreement with a similar observation in a recent study[4] involving only Czochralski-grown *i*-AlPdMn samples.

When relating the electrical and magnetic response of the three investigated *i*-AlPdMn samples to their structural perfection, we can make the following conclusions. X-ray analysis (Fig. 1) shows that all three samples are of high and comparable structural quality. A small difference in the diffraction peak widths indicates a slightly smaller amount of phason disorder in the two Czochralski-grown samples as compared to the flux-grown f-$AlPdMn_{8.5}$. No clear distinction between the structural qualities of the two Czochralski samples can be made on this basis, except for the fact that

the intensity match of the x-ray lines of the sCz-$AlPdMn_{8.3}$ sample to the reference sample[15] is slightly better than that of the Cz-$AlPdMn_{8.3}$. According to this, there exists a qualitative indication that the superannealed sCz-$AlPdMn_{8.3}$ sample could be structurally the most perfect and the f-$AlPdMn_{8.5}$ contains slightly more phason disorder than the two Czochralski samples. One should, however, keep in mind that all three samples are of high quality and that the differences in their structural perfection are not large. The often-claimed correlation between the structural perfection and the magnetic and electrical response of QC's, i.e., that higher resistive and less magnetic samples are structurally more perfect, is still qualitatively supported by our results, though it does not appear obvious for high-quality QC's. Such a trend may be anticipated for samples of medium and poor quality that exhibit considerable disorder in the QC lattice and possibly contain secondary phases, either periodic or quasiperiodic. Such degradation of the long-range quasiperiodic order certainly acts to recover and increase the metallic character of the QC's, but these effects are *extrinsic* to the quasiperiodicity.

In our study, the lowest-resistive and strongest-magnetic f-$AlPdMn_{8.5}$ sample is structurally not much different from the two Czochralski samples, yet its $\rho(T)$ and $\chi(T)$ properties are considerably different and show trends normally attributed to ''bad'' QC's. Anticipating that the observed tiny differences in the structural qualities of the three investigated *i*-AlPdMn samples could be at the origin of their different electrical and magnetic response, then even a minute amount of disorder could play a critical role in the magnetic and transport properties of QC's. With this in mind, it is fair to say that the magnetic ground state and the electrical conductivity intrinsic to the quasiperiodicity of the *i*-AlPdMn QC's need further consideration by performing experiments on defect-free single-phase and single-grain samples of further improved structural quality and grown by different techniques.

V. CONCLUSIONS

The electrical resistivity, magnetic susceptibility, and partial *s*-state DOS physical parameters of the three investigated *i*-AlPdMn QC's show significant differences, despite their comparable XRD-determined structural qualities. The Czochralski-grown samples were found to be less magnetic and more resistive than the self-flux-grown sample. The larger amount of magnetic Mn atoms correlates with the increased metallic character of the samples. Though our results are in qualitative agreement with the previously observed empirical trend that high resistivity is associated with high structural quality of the *i*-AlPdMn QC's, the small differences in the structural perfection of the investigated samples do not give convincing support to the hypothesis that this could be the main origin of the large differences in the electrical and magnetic response between the investigated samples. The ambiguity, whether high resistivity is associated with high structural quality, has also been raised in similar experiments on flux-grown *i*-AlPdMn samples[12] as well as for some other QC families such as[14] the *i*-AlPdRe and the rare-earth-containing[32] i-ZnMgR, where R denotes a rare-earth metal. Our study, which combines results of Czochralski- and flux-grown *i*-AlPdMn samples, cannot discard this ambiguity.

We have shown that even in the case of high-quality samples of comparable structural order, the electrical resistivity, the electronic DOS at E_F, and the number of magnetic Mn atoms differ considerably. As these physical parameters have a profound effect on the magnetic and transport properties of QC's, it is not surprising that such a large variety of very diverse physical phenomena were reported so far in the literature for differently prepared *i*-AlPdMn samples.

ACKNOWLEDGMENT

We thank Professor I. R. Fisher from Stanford for provision of the flux-grown f-$AlPdMn_{8.5}$ sample.

[1] M. A. Chernikov, A. Bernasconi, C. Beeli, A. Schilling, and H. R. Ott, Phys. Rev. B **48**, 3058 (1993).
[2] J. C. Lasjaunias, A. Sulpice, N. Keller, J. J. Préjean, and M. de Boissieu, Phys. Rev. B **52**, 886 (1995).
[3] V. Simonet, F. Hippert, M. Audier, and G. Trambly de Laissardière, Phys. Rev. B **58**, R8865 (1998).
[4] J. J. Préjean, C. Berger, A. Sulpice, and Y. Calvayrac, Phys. Rev. B **65**, 140203(R) (2002).
[5] P. Lanco, T. Klein, C. Berger, F. Cyrot-Lackmann, G. Fourcaudot, and A. Sulpice, Europhys. Lett. **18**, 227 (1992).
[6] H. Akiyama, T. Hashimoto, T. Shibuya, K. Edagawa, and S. Takeuchi, J. Phys. Soc. Jpn. **62**, 939 (1993).
[7] M. Rodmar, B. Grushko, N. Tamura, K. Urban, and Ö. Rapp, Phys. Rev. B **60**, 7208 (1999).
[8] R. Escudero, J. Lasjaunias, Y. Calvayrac, and M. Boudard, J. Phys.: Condens. Matter **11**, 383 (1999).
[9] T. Klein, C. Berger, D. Mayou, and F. Cyrot-Lackmann, Phys. Rev. Lett. **66**, 2907 (1991).
[10] H. Fukuyama and K. Hoshino, J. Phys. Soc. Jpn. **50**, 2131 (1981).
[11] J. Dolinšek, M. Klanjšek, Z. Jagličić, A. Bilušić, and A. Smontara, J. Phys.: Condens. Matter **14**, 6975 (2002).
[12] I. R. Fisher, M. J. Kramer, T. A. Wiener, Z. Islam, A. R. Ross, T. A. Lograsso, A. Kracher, A. I. Goldman, and P. C. Canfield, Philos. Mag. B **79**, 1673 (1999).
[13] I. R. Fisher, M. J. Kramer, Z. Islam, T. A. Wiener, A. Kracher, A. R. Ross, T. A. Lograsso, A. I. Goldman, and P. C. Canfield, Mater. Sci. Eng., A **294–296**, 10 (2000).
[14] I. R. Fisher, X. P. Xie, I. Tudosa, C. W. Gao, C. Song, P. C. Canfield, A. Kracher, K. Dennis, D. Abanoz, and M. J. Kramer, Philos. Mag. B **82**, 1089 (2002).
[15] S. Matsuo, H. Nakano, T. Ishimasa, and M. Mori, J. Phys. Soc. Jpn. **62**, 4044 (1993).
[16] A. Smontara and C. Beeli (unpublished).
[17] F. E. Mabbs and D. J. Machin, *Magnetism and Transition Metal Complexes* (Chapman and Hall, London, 1973), p. 7.
[18] J. H. Van Vleck, *The Theory of Electrical and Magnetic Suscep-*

tibilities (Oxford, London, 1952), p. 285.
[19] J. Dolinšek, M. Klanjšek, T. Apih, A. Smontara, J. C. Lasjaunias, J. M. Dubois, and S. J. Poon, Phys. Rev. B **62**, 8862 (2000).
[20] J. Dolinšek and M. Klanjšek, Phys. Rev. B **63**, 134203 (2001).
[21] T. Apih, O. Plyushch, M. Klanjšek, and J. Dolinšek, Phys. Rev. B **60**, 14 695 (1999).
[22] X. P. Tang, E. A. Hill, S. K. Wonnell, S. J. Poon, and Y. Wu, Phys. Rev. Lett. **79**, 1070 (1997).
[23] E. A. Hill, T. C. Chang, Y. Wu, S. J. Poon, F. S. Pierce, and Z. M. Stadnik, Phys. Rev. B **49**, 8615 (1994).
[24] A. Abragam, *The Principles of Nuclear Magnetism* (Oxford University Press, London, 1961), p. 385.
[25] A. Narath, Phys. Rev. **162**, 320 (1967).
[26] J. J. Spokas and C. P. Slichter, Phys. Rev. **113**, 1462 (1959).
[27] A. Quandt and V. Elser, Phys. Rev. B **61**, 9336 (2000).
[28] E. S. Zijlstra and S. K. Bose (unpublished).
[29] O. K. Andersen, Phys. Rev. B **12**, 3060 (1975).
[30] O. K. Andersen and O. Jepsen, Phys. Rev. Lett. **53**, 2571 (1984).
[31] D. A. Papaconstantopoulos, *Handbook of the Band Structure of Elemental Solids* (Plenum, New York, 1986), p. 208.
[32] I. R. Fisher, Z. Islam, A. F. Panchula, K. O. Cheon, M. J. Kramer, P. C. Canfield, and A. I. Goldman, Philos. Mag. B **77**, 1601 (1998).